RSC Advances

ROYAL SOCIETY OF CHEMISTRY

www.rsc.org/advances

Journal Name RSCPublishing

ARTICLE

3D Porous interconnected $NaVPO_4F/C$ network: Preparation and performance for Na-ion battery

Cite this: DOI: 10.1039/x0xx00000x

Received 00th January 2012,
Accepted 00th January 2012

DOI: 10.1039/x0xx00000x

www.rsc.org/

Maowen Xu[a,b,] †*, Chuan-Jun Cheng[a,b],†, Qiang-Qiang Sun[a,b], Shu-Juan Bao[a,b],Yu-Bin Niu[a,b], Hong He[a,b], Yutao Li[c] , Jie Song[c]

Uniform carbon embedded nano-scaled $NaVPO_4F$ precursor with 3~5 nm is fabricated by a hydrothermal method and using vitamin C as the carbon source and reducing agent, followed a sintering process, the carbon embedded $NaVPO_4F$ precursors transformed to a kind of 3D porous interconnected $NaVPO_4F/C$ network. As a Na-ion battery cathode material, the $NaVPO_4F/C$ network obtained at 750 ^oC achieves a high discharge capacity of 121 mAh g^{-1} and the obtained sample at 800 ^oC shows a little lower discharge capacity of 101 mAh g^{-1}, but better rate capability and long life cycles. These results indicate that the 3D porous $NaVPO_4F/C$ network not only improves electronic conductivity of active material, but prevents the aggregation of particles, and its open porous structure allows electrolyte penetration, and reduces the diffusion path of the sodium ions, hence maximizes utilization of the electrochemically active $NaVPO_4F$ particles.

Introduction

Energy storage and conversion technology is widely used in portable electronics products, and this technology is gaining worldwide attention for its transportation applications and other large-scale renewable energy storage equipments[1-3]. Among the candidates, despite the popularity of Li-ion batteries in energy storage applications, their relatively high cost and the geographic constraints associated with lithium resources have motivated a search for cheaper and more sustainable alternatives[4-6]. In comparison, sodium resources are inexhaustible and unlimited everywhere around the world. After lithium, the electrochemical equivalent and standard potential of sodium are the most advantageous for aprotic battery applications; therefore, sodium-ion batteries are receiving widespread attentions[7-9]. However, only a limited number of successful candidates are found for sodium insertion as cathode materials compared to that for lithium ion battery.

Recently, some layered compounds and F-containing V-based polyanion compounds have been investigated as possible cathode materials for Na-ion batteries, such as Na_xMO_2 (M = V, Co, Mn, Fe)[10-13], $NaVPO_4F$[14], $Na_3V_2O_2(PO_4)_2F$[15], $Na_3V_2(PO_4)_2F_3$[16], and $Li_{1.1}Na_{0.4}VPO_{4.8}F_{0.7}$[17]. Among these candidates, $NaVPO_4F$ recently attracts extensive attention because of its high theoretical specific capacity of 143 mAh g^{-1} and its open framework structure[18]. $NaVPO_4F$ with a tetragonal structure was firstly proposed by J. Barker et al.[18], and various methods were introduced to prepare $NaVPO_4F$, including two-step solid state reaction, hydrothermal approach and sol–gel synthesis[18-20]. However, the capacity of the reported $NaVPO_4F$ materials is far below its theoretical specific capacity and show bad cycling performance.

Carbon coating is an effective approach to increase the electronic conductivity and electrochemical performance of the cathode materials[21-23]. There are many studies on enhancing the overall

performance of cathode materials by carbon coating and different synthesis methods. Designing a porous network is another effective strategy for improving the performance of the electrode owing to favorable electrolyte absorption and significant reduction of sodium-ion diffusion paths[24]. Herein, we report a novel approach to synthesize $NaVPO_4F$/C network which consists of nanoparticles and microparticles with open interconnected 3D porous microstructure. As shown in Fig. 1, the $NaVPO_4F$/C precursor obtained by dropping absolute alcohol to $NaVPO_4F$ precursor solution and following by hydrothermal reaction consisted of uniformed nanoparticles and completely coated with carbon. After calcination, the embedded nanosize $NaVPO_4F$ grew up and aggregated together and outer carbon layer played an important role in forming the 3D porous interconnected $NaVPO_4F$ network. This simple approach could be extended to other battery materials to obtain improved electrochemical performance.

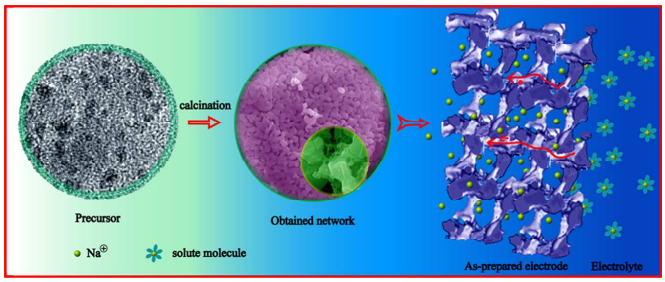

Fig. 1 Schematic of design and fabrication of three-dimensional $NaVPO_4F$/C network and electron and ion transfer pathway inside $NaVPO_4F$/C network.

Experimental

Material preparation

2 mmol NH_4VO_3 and 2 mmol NaF were dissolved into 10 mL deionized water under stirring at 80 °C in a 100 mL beaker. 2 mmol $NH_4H_2PO_4$ and 3 mmol vitamin C were dissolved into 10 mL deionized water, and then slowly dropped into the above solution under continuous stirring. Subsequently a blue solution was obtained. Then 50 mL absolute alcohol was added to this mixed solution and kept continuous stirring for 0.5 h. The as obtained blue suspension was transferred into two separate 50 mL Teflon autoclaves .The autoclaves were sealed, kept at 180 °C for 24 h, and then cooled to room temperature naturally. The as-synthesized precipitate was collected by centrifugation and frozen dried to get a black brown precursor. Finally, the prepared precursors were calcined at 750 °C and 800 °C for 6 h under argon, respectively. The samples sintered at 750 °C and 800 °C were denoted as $NaVPO_4F$-750 and $NaVPO_4F$-800, respectively. Similarly, In order to optimize the reaction conditions， the samples were prepared in different times and under different temperatures.

Material characterization

The crystal structure of the products was characterized by X-ray diffraction (XRD-7000). Morphology and microstructure of the synthesized materials was investigated by field emission scanning electron microscopy (JSM-6700F, Japan) and transmission electron microscopy (JEM-2010, Japan). The carbon content was tested by CHNOS elemental analysis (vario EL CUBE, Germany).

Electrode fabrication and electrochemical tests

To evaluate the electrochemical performance of the as-prepared sample, CR2032-type coin cells were fabricated in an argon-filled glove box. This coin cell was composed of sodium anode, cathode, Celgard polypropylene separator, and 1 M $NaPF_6$ solution in a mixture of ethylene carbonate (EC) and diethyl carbonate (DEC) (EC/DEC, 1:1 v/v) as the electrolyte. The cathode was prepared by spreading the slurry of the active material (80 wt%), carbon black (10 wt%) and the poly(vinylidene fluoride) (10 wt%) binder dissolved in N-methyl pyrolidine on Al foil. The working electrolytes were dried in vacuum at 120 °C for overnight. The loading of the active material ($NaVPO_4F$/C) was about 2~3 mg cm^{-2}. The assembled cells were rested for 24 h prior to further testing in order to ensure full absorption of the electrolyte into the working

electrode. Charge-discharge tests were performed at room temperature with an Arbin.

Results and Discussion

The XRD patterns of the as-synthesized samples display in Fig.2. In order to optimize the reaction conditions, some experiments were done in different react times and temperatures (See Fig.S1 and Fig.S2).The pattern of Fig.2a suggests the precursor obtained in hydrothermal reaction at 180 °C for 24 h has a tetragonal symmetry structure (space group *I*4/*mmm*). VO_4F_2 octahedra and PO_4 tetrahedra stack an extended three-dimensional framework. The position of its diffraction peaks agrees with the previous work published by Barker et al[18, 19]. However, the intensity of its diffraction peaks embodies the characteristics of amorphous

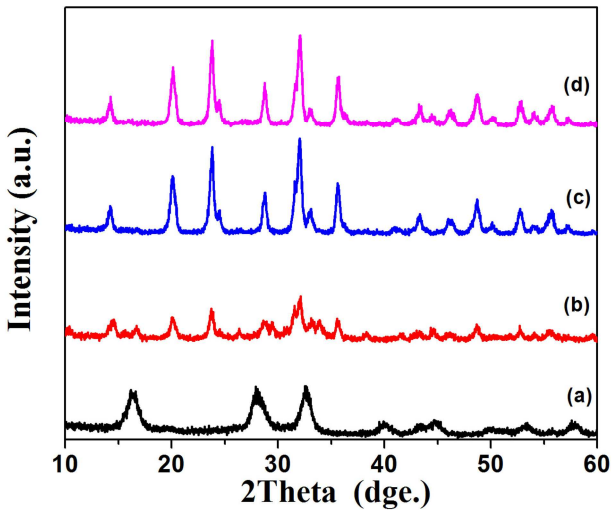

Fig. 2 XRD patterns of $NaVPO_4F$/C composites (a) Hydrothermal method at 180 °C for 24 h, (b) Precursor after calcined at 700 °C for 6 h, (c) Precursor after calcined at 750 °C for 6 h.

materials. After sintering at 750 °C and 800 °C, the XRD results (Fig.2c and d) are in good agreement with that reported by Zhou et al.[14, 20, 25], suggesting the phase of monoclinic crystal (space group C2/c), two PO_4 tetrahedra share two corner-oxygen atoms with two different VO_4F_2 octahedra. While the product formed at 700 °C is a mixed phase of tetragonal structure and monoclinic crystal (Fig.2b).

$NaVPO_4F$ have been conventionally synthesized by hydrothermal method or the two-step solid state. The reaction intermediate phase is VPO_4, prefabricated by the high temperature carbon-thermal reduction reaction[18]. In this work, we first prepare uniformly carbon embedded nano-scaled $NaVPO_4F$ precursors by a feasible and environmentally friendly hydrothermal method utilizing vitamin C as both the carbon sources and the reducing agent. And then further to sinter the obtained precursors at high temperature to form 3D porous interconnected $NaVPO_4F$/C network. The unique architecture of the $NaVPO_4F$/C precursor used in our work is displayed in Fig.3. It is clear that the precursor is very uniform nanoparticles, the $NaVPO_4F$ nanoparticles with diameters of 3~5 nm are embedded in the carbon matrix.

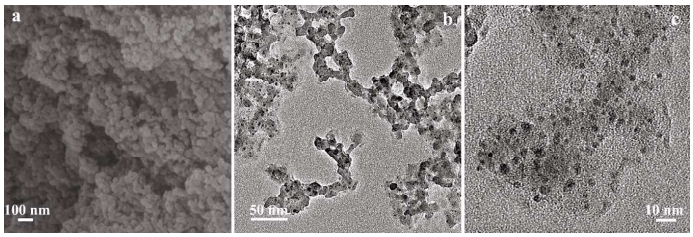

Fig. 3 SEM (a) and TEM (b and c) of carbon embedded $NaVPO_4F$ obtained at hydrothermal process.

The product sintered at 750 °C displays 3D interconnected network structure composed of uniform particles (Fig. 4a). These grown particles are connected together and disordered carbon distribute between these big particles (Fig. 4b and c). $NaVPO_4F$ sintered at 750 °C, which is coated by fine amorphous carbon coating layers, displayed clear crystal planes (Fig. 4d). The thickness of the carbon layer is about ~5 nm (Fig. 4d). The carbon embedded $NaVPO_4F$ precursor can prevent the aggregation of $NaVPO_4F$ particles, and help to form porous interconnected network structure. For the

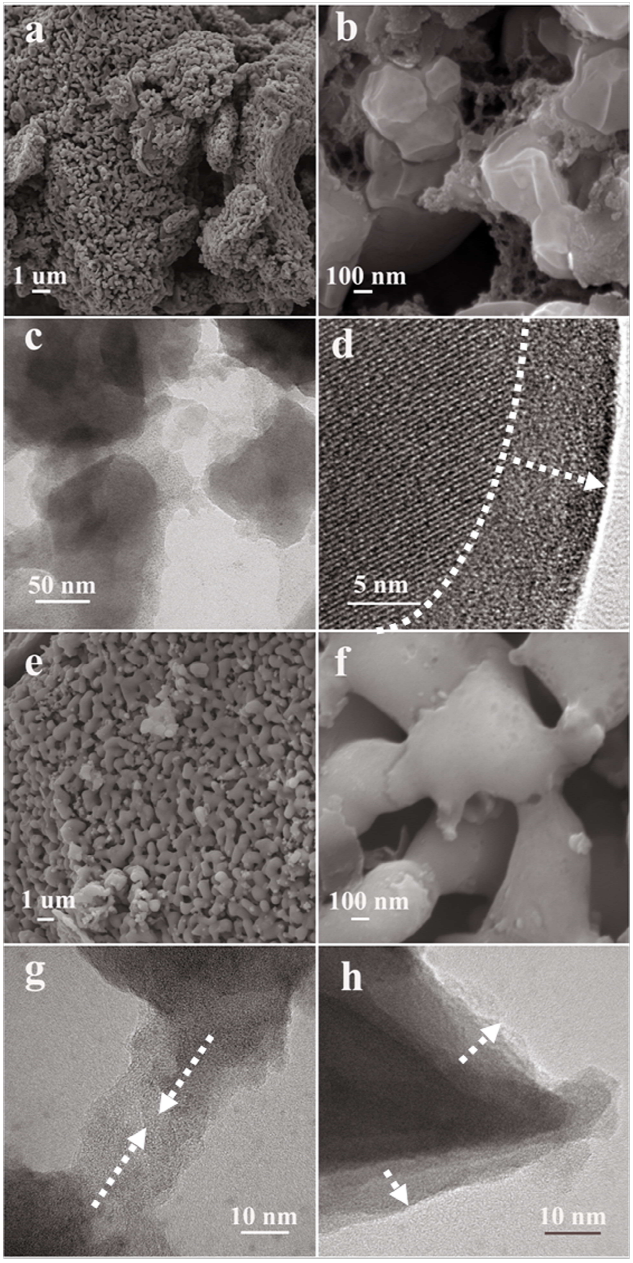

Fig. 4 SEM and TEM of $NaVPO_4F/C$ composites obtained at different temperatures. (a to d) 750 °C and (e to h) 800 °C.

$NaVPO_4F$ samples fired at 800 °C, the particle size is in the range of 1–3 μm; these microparticles interweave together forming an open porous structure. (Fig. 4e and f). These coating carbon on $NaVPO_4F$ nanoparticles create a carbon network and improve the electronic conductivity, the width of bridge-like carbon is about 10~50 nm (Fig. 4g and h). Such a well-organized 3D interconnected network structure facilitates the electrolyte penetration into the $NaVPO_4F$ particles and provides more interface area between the electrolyte and the electrode material. The carbon content in $NaVPO_4F/C$ precursors, $NaVPO_4F/C$ sintered at 750 °C and 800 °C are estimated by elemental analysis. The results showed that the carbon content is about 9.6 wt%, 2.9 wt% and 1.4 wt% of the samples by hydrothermal method, sintered at 750 °C and 800 °C, separately. In additional, as shown in the Fig. S3, 4 and 5, the energy dispersive spectrometer (EDS) mapping shows no impurity elements. All five elements –Na, V, P, O and F are present uniformly throughout the bulk of the sample.

In order to examine the potential application of NaVPO4F/C network in sodium ion batteries, the electrochemical properties of $NaVPO_4F/C$ composite were tested in the coin half-cells at room temperature in the voltage range of 2.5~4.2 V. Fig. 5a shows the cyclic voltammograms of the obtained composites at a scan rate of 0.1 mV s^{-1}. It is seen that the $NaVPO_4F$ precursor obtained during hydrothermal process shows unobvious peaks and the redox couple is at around 3.55 V/3.65 V. And one wide redox couple (3.1 V/3.5 V) can be observed for the $NaVPO_4F$ sintered at 750 °C. When the sintering temperature increases to 800 °C, two redox couples at 3.15 V/3.45 V and 3.6 V/3.7 V can be identified. Fig. 5b illustrates the typical first cycle profiles of charge–discharge curves at 0.1C (corresponds to 14.3 mA g^{-1}). The charge and discharge plateaus of $NaVPO_4F$ materials agree with the CV results. Because of different phases, the redox potential of $NaVPO_4F$ precursor is about 0.5 V higher than that of the samples obtained by sintered at high temperature. The specific capacity of $NaVPO_4F/C$ composites (hydrothermal, 750 °C and 800 °C) are 50 mAh g^{-1}, 121 mAh g^{-1} and 101 mAh g^{-1}, respectively,. Due to the looser surface structure and higher carbon content, the $NaVPO_4F/C$ sintered at 750 °C exhibits a better specific capacity than the $NaVPO_4F/C$ sintered at 800 °C. The rate performances of $NaVPO_4F/C$ composite (hydrothermal, 750 °C and 800 °C) at various rates from 0.1 C to 1 C are illustrated in Fig 5c. The as-synthesized $NaVPO_4F$-750 demonstrates a good rate capability at rate 0.1 C, 0.2 C and 0.5C (i.e., the tenth capacities of

$NaVPO_4F$-750 and $NaVPO_4F$-800 are 115 and 97 mAh g^{-1} at 0.1C, the twentieth capacities of $NaVPO_4F$-750 and $NaVPO_4F$-800 are 107 and 90 mAh g^{-1} at 0.2 C, the thirtieth capacities of $NaVPO_4F$-750 and $NaVPO_4F$-800 are 91 and 83 mAh g^{-1} at 0.5 C), which is far higher than that of the $NaVPO_4F$/C (97.8 mA h g^{-1} at 0.1C and 99.1mA h g^{-1} at 0.1C) fabricated by Y. Lu et al[14] and Y.-L. Ruan et al[26]. It is interesting to find that the capacities of the as-synthesized $NaVPO_4F$-750 and $NaVPO_4F$-800 are basically equal (about 78 mAh·g^{-1}) at 1C. Fig. 5d further compared the cycle stability of these samples, and the discharge capacity of hydrothermal $NaVPO_4F$ precursor decreases from 46 mAh·g^{-1} to only 14 mAh·g^{-1} after 65 cycles, while the $NaVPO_4F$-750 and $NaVPO_4F$-800 show good capacity retention, their discharge capacities reduce from 121 to 92 mAh·g^{-1} and from 101 to 83 mAh·g^{-1} after 65 cycles.

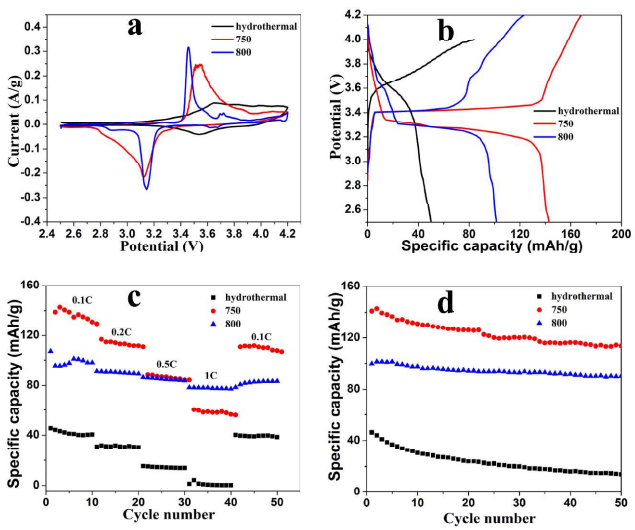

Fig. 5 The electrochemical properties of $NaVPO_4F$ precursor and $NaVPO_4F$ sintered at 750 °C and 800 °C :(a) cyclic voltammograms at a scan rate of 0.1 mV·s^{-1}; (b) the typical first cycle profiles of charge–discharge curves at 0.1 C; (c) performance at various rates from 0.1 C to 1 C; (d) cycle performances at 0.1 C.

Conclusion

In this study, a kind of 3D porous interconnected $NaVPO_4F$/C network was prepared by using carbon embedded nano-scaled $NaVPO_4F$ as precursor. The carbon embedded $NaVPO_4F$ precursor can prevent the aggregation of $NaVPO_4F$ particles, and help to form porous interconnected network structure. The unique 3D network structure provides interconnected open pores and effectively carbon coating, which allows electrolyte penetration, improves the electronic conductivity and reduces the diffusion path of the sodium ions. The results indicate that $NaVPO_4F$/C network delivered a high discharge capacity and a good long-term cycling life. This novel method could be extended to obtain various porous materials for use in energy storage and conversion, as well as catalysis.

Acknowledgments

This work is financially supported by Chongqing Key Laboratory for Advanced Materials and Technologies of Clean Energies under cstc2011pt-sy90001, Start-up grant under SWU111071 from Southwest University and Chongqing Science and Technology Commission under cstc2012gjhz90002. The work is also supported by grants from the National Natural Science Foundation of China (No. 21063014, 21163021), Fundamental Research Funds for the Central Universities (SWU113079, XDJK2014C051) and Research Funds for a postdoctor of Chongqing（xm2014097）

Notes and references

[a] *Institute for Clean Energy & Advanced Materials, Faculty of Materials and Energy， Southwest University, Chongqing 400715, P.R. China*
[b] *Chongqing Key Laboratory for Advanced Materials and Technologies of Clean Energies, Chongqing 400715, P.R. China*
[c] *Texas Materials Institute, University of Texas at Austin, Texas 78712, USA*
† Maowen Xu and Chuan-Jun Cheng contributed equally to this work.
E-mail: xumaowen@swu.edu.cn

1. M. S. Whittingham, Chem. Rev, 2014, 114, 11414-11443.
2. J. Xie, C. X. Guo and C. Li, Energy Environ. Sci., 2014. 7, 2559-2579.
3. M. D. Slater, D. Kim, E. Lee and C. S. Johnson, Adv. Funct. Mater., 2013, 23, 947-958.
4. S. W. Kim, D. H. Seo, X. Ma, G. Ceder and K. Kang, Adv. Energy Mater., 2012, 2, 710-721.

5. M. Xu, L. Wang, X. Zhao, J. Song, H. Xie, Y. Lu and J. B. Goodenough, Chem. Chem. Phys., 2013, 15, 13032-13037.
6. J. Liu, K. Tang, K. Song, P. A. van Aken, Y. Yu and J. Maier, Nanoscale, 2014, 6, 5081-5086.
7. H. Pan, Y.-S. Hu and L. Chen, Energy Environ. Sci., 2013, 6, 2338-2360.
8. V. Palomares, M. Casas-Cabanas, E. Castillo-Martínez, M. H. Han and T. Rojo, Energy Environ. Sci., 2013, 6, 2312-2337.
9. W. Song, X. Ji, Z. Wu, Y. Yang, Z. Zhou, F. Li, Q. Chen and C. E. Banks, J. Power Sources, 2014, 256, 258-263.
10. M. Guignard, C. Didier, J. Darriet, P. Bordet, E. Elkaïm and C. Delmas, Nat. Mater., 2013, 12, 74-80.
11. R. Berthelot, D. Carlier and C. Delmas, Nat. Mater., 2011, 10, 74-80.
12. M. M. Doeff, M. Y. Peng, Y. Ma and L. De Jonghe, J. Electrochem. Soc., 1994, 141, L145-L147.
13. N. Yabuuchi, H. Yoshida and S. Komaba, Electrochemistry, 2012, 80, 716-719.
14. Y. Lu, S. Zhang, Y. Li, L. Xue, G. Xu and X. Zhang, J. Power Sources, 2014, 247, 770-777.
15. M. Xu, P. Xiao, S. Stauffer, J. Song, G. Henkelman and J. B. Goodenough, Chem. Mater. 2014, 26, 3089−3097.
16. Z. Liu, Y.-Y. Hu, M. T. Dunstan, H. Huo, X. Hao, H. Zou, G. Zhong, Y. Yang and C. P. Grey, Chem. Mater., 2014, 26, 2513-2521.
17. Y.-U. Park, D.-H. Seo, B. Kim, K.-P. Hong, H. Kim, S. Lee, R. A. Shakoor, K. Miyasaka, J.-M. Tarascon and K. Kang, Sci. Rep., 2012, 2.
18. J. Barker, M. Saidi and J. Swoyer, Electrochem. Solid-State Lett., 2003, 6, A1-A4.
19. J. Barker, M. Saidi and J. Swoyer, J. Electrochem. Soc., 2004, 151, A1670-A1677.
20. J. Zhao, J. He, X. Ding, J. Zhou, Y. o. Ma, S. Wu and R. Huang, J. Power Sources, 2010, 195, 6854-6859.
21. Y. Luo, X. Xu, Y. Zhang, Y. Pi, Y. Zhao, X. Tian, Q. An, Q. Wei and L. Mai, Adv. Energy Mater., 2014, 4.
22. Z. Yang, J. Xia, L. Zhi, W. Zhang and B. Pei, Ionics, 2014, 20, 169-174.
23. J. Wang, Z. Wang, X. Li, H. Guo, W. Xiao, S. Huang and Z. He, J. Solid-State Chem., 2013, 17, 1-8.
24. L. Dimesso, C. Förster, W. Jaegermann, J. Khanderi, H. Tempel, A. Popp, J. Engstler, J. Schneider, A. Sarapulova and D. Mikhailova, Chem. Soc. Rev., 2012, 41, 5068-5080.
25. H. Zhuo, X. Wang, A. Tang, Z. Liu, S. Gamboa and P. Sebastian, J. Power Sources, 2006, 160, 698-703.
26. Y.-L. Ruan, K. Wang, S.-D. Song, X. Han and B.-W. Cheng, Electrochim. Acta, 2015, 160, 330-336.